Title
Effects of deletion of the transcription factor Nrf2 and benzo [a]pyrene treatment on ovarian follicles and ovarian surface epithelial cells in mice

Authors
Lim, Jinhwan
Ortiz, Laura
Nakamura, Brooke N
et al.

Publication Date
2015-12-01

DOI
10.1016/j.reprotox.2015.07.080

Reproductive Toxicology 58 (2015) 24–32

Contents lists available at ScienceDirect

Reproductive Toxicology

journal homepage: www.elsevier.com/locate/reprotox

Effects of deletion of the transcription factor *Nrf2* and benzo [*a*]pyrene treatment on ovarian follicles and ovarian surface epithelial cells in mice

Jinhwan Lim[a], Laura Ortiz[a], Brooke N. Nakamura[a], Yvonne D. Hoang[a], Jesus Banuelos[a], Victoria N. Flores[a], Jefferson Y. Chan[c], Ulrike Luderer[a,b,*]

[a] Department of Medicine, University of California Irvine, USA
[b] Department of Developmental and Cell Biology, University of California Irvine, USA
[c] Department of Pathology and Laboratory Medicine, University of California Irvine, USA

ARTICLE INFO

Article history:
Received 13 April 2015
Received in revised form 29 June 2015
Accepted 31 July 2015
Available online 3 August 2015

Keywords:
NRF2
Ovarian aging
Benzo[a]pyrene
Oxidative stress
Polycyclic aromatic hydrocarbon
DNA adduct

ABSTRACT

Polycyclic aromatic hydrocarbons, like benzo[*a*]pyrene (BaP), are ubiquitous environmental pollutants and potent ovarian toxicants. The transcription factor NRF2 is an important regulator of the cellular response to electrophilic toxicants like BaP and to oxidative stress. NRF2 regulates transcription of genes involved in the detoxification of reactive metabolites of BaP and reactive oxygen species. We therefore hypothesized that *Nrf2*−/− mice have accelerated ovarian aging and increased sensitivity to the ovarian toxicity of BaP. A single injection of BaP dose-dependently depleted ovarian follicles in *Nrf2*+/+ and *Nrf2*−/− mice, but the effects of BaP were not enhanced in the absence of *Nrf2*. Similarly, *Nrf2*−/− mice did not have increased ovarian BaP DNA adduct formation compared to *Nrf2*+/+ mice. Ovarian follicle numbers did not differ between peripubertal *Nrf2*−/− and *Nrf2*+/+ mice, but by middle age, *Nrf2*−/− mice had significantly fewer primordial follicles than *Nrf2*+/+ mice, consistent with accelerated ovarian aging.

1. Introduction

Polycyclic aromatic hydrocarbons (PAHs) are ubiquitous environmental pollutants, which are formed during the incomplete combustion of organic materials. Tobacco smoke is rich in PAHs [1]. Inhalation exposure to PAHs also occurs in non-smokers, due to exposure to second hand tobacco smoke and to air pollution. PAHs in ambient urban air are more than 10-fold higher than in rural air [2,3]. Grilling or smoking of food also generates PAHs, and frequent consumption of grilled or smoked foods is another major source of PAH exposure [2,3].

Women who smoke have decreased per menstrual cycle probability of pregnancy compared to women who do not smoke [4–6] . The onset of menopause occurs several years earlier in women who smoke [7,8]. The adverse ovarian effects of smoking may be caused by PAHs present in tobacco smoke. The PAHs dimethylbenzanthracene (DMBA), 3-methylcholanthrene (3MC), and benzo[*a*]pyrene (BaP) all destroy follicles in mice after single high doses [9–12] and after repeated low doses [13] . DMBA also destroyed ovarian follicles in human ovarian explants, which were implanted subcutaneously in mice [14]. Prenatal and postnatal exposure to PAHs also causes ovarian tumors later in life [15,16]. We recently showed that prenatal exposure to BaP causes ovarian tumors, which exhibit high levels of the epithelial marker cytokeratin by immunostaining [17]. The latter results suggest that PAH-induced ovarian tumors may arise from the ovarian surface epithelial (OSE) cells from which most malignant ovarian tumors in women are believed to arise [18,19]. BaP has been shown to induce proliferation of mammary tumor cells in vitro [20–22], but effects of BaP on OSE cell proliferation in vivo have not been examined.

PAHs are oxidized by microsomal cytochrome P450 enzymes (chiefly P450s 1A1 and 1B1) to epoxides, which are converted to diols by microsomal epoxide hydrolase (*Ephx1*) [23,24]. Diols can undergo further oxidation by P450 enzymes to mutagenic and ovotoxic diol epoxides [23,25]. Alternatively, they can be metabolized by diol dehydrogenases, ultimately yielding catechols, which can undergo two sequential one-electron oxidations to *o*-semiquinone and then to *o*-quinone, generating hydrogen peroxide and superoxide anion radical [24]. The *o*-quinone can be reduced back to the semiquinone or catechol, resulting in redox cycles. All of the enzymes required to activate PAHs are present in the ovary [26–32].

* Corresponding author at: Center for Occupational and Environmental Health, 100 Theory Drive, Suite 100, Irvine, CA 92617, USA.
E-mail address: uluderer@uci.edu (U. Luderer).

http://dx.doi.org/10.1016/j.reprotox.2015.07.080
0890-6238/

Glutathione-*S*-transferase (GST)-catalyzed conjugation with glutathione (GSH) is an important Phase II detoxification mechanism for the diol epoxide, diol, and quinone metabolites of PAHs [33], and GSH also reduces and detoxifies reactive oxygen species (ROS) via direct reactions or as a cofactor for glutathione peroxidases.

The Cap 'n Collar basic leucine zipper transcription factor nuclear factor 2 erythroid related factor 2 (NRF2) regulates transcription of GSTs, the enzymes of GSH synthesis, superoxide dismutase, NADPH quinone oxidoreductase, and UDP-glucuronosyltransferase, which are important in detoxifying PAH metabolites and ROS, and of *Ephx1*, which is required to generate ovotoxic metabolites of PAHs [34–36]. *Nrf2* null mice are more susceptible than wild type mice to chemical toxicity, including cancer induction by the PAH BaP [37], ovarian toxicity by vinylcyclohexene diepoxide [38], and liver toxicity by acetaminophen [39] . They are also more susceptible to autoimmune diseases [40,41] than wild type mice. *Nrf2*−/− mice also exhibit increased oxidative stress compared to *Nrf2+/+* mice [42]. We previously reported that young male *Nrf2*−/− mice had normal spermatogenesis, but developed age-related defects in spermatogenesis compared to wild type littermates, which was associated with increased testicular oxidative lipid damage [43]. We and others have shown that oxidative stress is associated with normal ovarian aging [44–46] and that deletion of the antioxidant gene *Gclm* causes accelerated ovarian aging [47].

Herein we report on the results of experiments testing the hypotheses that (1) *Nrf2*−/− mice are more sensitive to ovarian DNA damage, apoptosis, and follicle destruction by BaP than *Nrf2+/+* mice due to their decreased ability to detoxify reactive metabolites of BaP; (2) BaP stimulates OSE cell proliferation and this occurs to a greater extent in *Nrf2*−/− ovaries than in *Nrf2+/+* ovaries; (3) *Nrf2* deletion accelerates the age-related decline in ovarian follicle numbers.

2. Methods

2.1. Materials

All chemicals and reagents were purchased from Sigma–Aldrich (St. Louis, MO) or Fisher Scientific (Pittsburgh, PA), unless otherwise noted.

2.2. Animals

Nrf2 null mice were generated by disrupting the *Nrf2* gene by homologous recombination in embryonic stem cells, using a targeting vector that results in deletion of part of exon 4 and all of exon 5, replacing them with a *LacZ* reporter gene [48] . Mice for these experiments were generated in our breeding colony by mating *Nrf2+/−* males with *Nrf2+/−* females. *Nrf2+/−* breeder mice had been backcrossed 8 times onto a C57BL/6Crl genetic background. Genotyping of tail snip DNA by PCR was carried out as described [48]. The mice were housed in an American Association for the Accreditation of Laboratory Animal Care-accredited facility, with free access to deionized water and laboratory chow (Prolab RMH 2500), on a 14:10 h light–dark cycle. Temperature was maintained at 21–24 °C. Experimental females were group-housed with their female littermates after weaning (up to 5 mice per cage). The experimental protocols were carried out in accordance with the *Guide for the Care and Use of Laboratory Animals* [49] and were approved by the Institutional Animal Care and Use Committee at the University of California Irvine.

2.3. Experimental protocol—ovarian effects of BaP treatment in *Nrf2+/+* and *Nrf2*−/− mice

To investigate the effects of lack *Nrf2* on the ovarian sensitivity to BaP, 28-day old *Nrf2*−/− and *Nrf2+/+* female mice were injected intraperitoneally with 0, 2, or 50 mg/kg BaP dissolved in sesame oil ($N = 5$ to 9/group). These doses were chosen based on a prior study, which showed that a single dose of 50 mg/kg depleted primordial follicles by 56%, while a 5 mg/kg dose depleted primordial follicles by 18% [12]. Seven days later at 35 days of age, mice were euthanized using carbon dioxide inhalation. One ovary per animal was randomly chosen for fixation in Bouin's fixative for 24 h, followed by 4 washes in 50% ethanol, and storage in 70% ethanol. The other ovary was fixed in 4% paraformaldehyde (PFA) in PBS for 1 h, then cryoprotected in 15% sucrose in PBS for 4 h prior to being embedded in Tissue-Tek OCT (Sakura Finetek, Torrance, CA). The embedded ovaries were serially sectioned at 10 μm for immunohistochemistry and terminal deoxynucleotidyl transferase dUTP nick end labeling (TUNEL). Another set of mice was treated identically with 0 or 50 mg/kg BaP, and both ovaries were snap frozen on dry ice for subsequent DNA extraction for ^{32}P-postlabeling to detect BaP-related DNA adducts.

2.4. GSH assays

For GSH assays, ovaries from 6 *Nrf2+/+* and 7 *Nrf2*−/− 18–22 day old mice were homogenized in 20 mM Tris, 1 mM EDTA, 250 mM sucrose, 2 mM L-serine, 20 mM boric acid (TES-SB). After removal of aliquots for protein assay, supernatants were acidified with one quarter volume 5% sulfosalicylic acid for GSH assays [50]. Total GSH was measured using a modification of an enzymatic recycling assay developed by Griffith [50–52]. Triplicates of samples or standards were combined with 33 μl metal free water and incubated for 10 min at 30 °C. The samples were mixed with 140 μl of 0.3 mM NADPH, 20 μl of 6 mM DTNB (5,5′-dithiobis) (2-nitrobenzoic acid), and 2 μl of 50 units/mL GSH reductase. The rate of thiobis(2-nitrobenzoic acid) (TNB) formation from DTNB is proportional to the total GSH concentration in each sample. TNB formation was monitored by measuring the absorbance at 412 nm for 5 min every 10 s using a VersaMax microplate spectrophotometer (Molecular Devices, Sunnyvale, CA). The concentrations of total GSH in the samples were calculated from a standard curve generated from the slopes of the standards.

2.5. Immunoblotting for GCLC, GCLM, SOD2 in ovarian extracts

Ovaries from 34 to 36 day old *Gclm*−/− and *Gclm+/+* littermates were homogenized in RIPA buffer (PBS, 0.5% sodium deoxycholate, 0.1% SDS, 1% NP40) with protease inhibitors (Pefablock, TLCK, pepstatin, aprotonin, leupeptin) using a Kontes handheld dounce homogenizer (Kimble-Chase, Vineland, NJ) on ice. Protein concentration was determined by Pierce BCA (bicinchoninic acid) Assay. Twenty to forty micrograms of each protein sample were separated by SDS-PAGE, transferred to polyvinylidine difluoride membranes, blocked in 5% nonfat milk in phosphate buffered saline with 0.1% Tween-20, incubated with primary antibodies diluted in 3% nonfat dry milk, 3% BSA, 1% ovalbumin, 1% normal goat serum, 0.1% sodium azide, and then visualized with ECL chemiluminescence (GE Healthcare Lifesciences, Piscataway, New Jersey). GCL subunit antibodies were raised against ovalbumin conjugates and were a kind gift of Dr. Terrance J. Kavanagh, University of Washington [53]. GCLC subunit antibodies were used at a dilution of 1:40,000 and GCLM at 1:20,000. Antibody directed against manganese containing superoxide dismutase (SOD2) was purchased from Stressgen (#SOD-110, Ann Arbor, MI) and used at a 1:5000 dilution. All immunoblots were re-probed with monoclonal anti-β-actin mouse

antibody (Sigma, #A5441) at a 1:160 K dilution for normalization of protein loading.

2.6. Quantitative real time RT-PCR

For quantitative real time RT PCR, total RNA was extracted from ovaries of 27 day old mice using the Qiagen RNEasy Mini Kit (Qiagen, Valencia, CA) according to the manufacturer's instructions. The quality and quantity of the total RNA were assessed by spectrometry. Purified total RNA (900 ng) was reverse-transcribed to cDNA with Superscript II reverse transcriptase (Invitrogen, Carlsbad, CA) using an oligo $dT_{12–18}$ primer (Invitrogen) after digestion with DNAse I (Roche, Indianapolis, IN). Twenty nanograms of cDNA were subjected to PCR using gene-specific forward and reverse primers and the Roche SYBR Green RT-PCR reagent (Roche) in 20 μl reaction volumes in duplicate. Gene-specific primers used are listed in Supplemental Table S1. The PCR amplification of all transcripts was performed on the AB StepOne Plus PCR machine (Applied Biosystems, Foster City, CA) using the following program: (1) initial incubation at 95 °C for 10 min to activate FastStart Taq DNA polymerase; (2) each cycle (total 40 cycles) at 95 °C for 10 s, followed by incubation at an average annealing temperature of forward and reverse primers for 30 s according to the primers used, and final elongation at 72 °C for 10 s. The quality and identity of each PCR product was determined by melting curve analysis. Expression of each target gene was calculated by the delta–delta Ct method [54,55]. All data were normalized to expression of glyceraldehyde-3-phosphate dehydrogenase (*Gapdh*).

2.7. Ovarian histomorphometry

In addition to ovaries from 35 day old *Nrf2+/+* and *Nrf2−/−* mice treated with BaP or vehicle, ovaries were harvested on the day of estrus from 10 and 12 month old, untreated *Nrf2+/+* and *Nrf2−/−* mice. After fixation with Bouin's fluid, ovaries were embedded in paraffin and complete serial sections (6 μm thick) were cut. Sections were stained with hematoxylin and eosin. Histomorphometry was carried out by a skilled observer, blind to genotype and BaP dose. Follicles were classified as primordial (oocyte surrounded by single layer of fusiform granulosa cells), primary (oocyte surrounded by single layer of granulosa cells of predominantly cuboidal morphology), secondary (oocyte surrounded by more than one layer of granulosa cells), or antral (follicle with multiple fluid-filled vesicles or single antrum) according to established criteria [56–58]. Follicles were also classified as healthy or atretic according to established criteria [59,60]. Healthy and atretic primordial, primary, and secondary follicles were counted in every 5th section. Healthy and atretic antral follicles were counted in every section, Only secondary and antral follicles in which the oocyte nucleolus was visible were counted to avoid overcounting. Multiovular follicles (follicles with more than one oocyte) of all stages were identified and counted.

2.8. ^{32}P postlabeling

DNA was extracted from ovaries and purified using a Qiagen DNeasy Tissue Kit (Qiagen, Valencia, CA). ^{32}P-postlabeling for detection of BaP DNA adducts was performed according to previously described methods [61–63]. Five micrograms of the purified DNA was dried using a Speedvac evaporator. Digestion of DNA was accomplished by incubation in hydrolysis buffer, micrococcal nuclease, and spleen phosphodiesterase for 3.5 h at 37 °C. To the digested material was added $ZnCl_2$, sodium acetate, and nuclease P1, which was used to separate adduct nucleotides from normal nucleotides. This incubation was performed for 1 h at 37 °C. Addition of Tris base was then performed, followed by preparation of a labeling mixture consisting of kinase buffer, polynucleotide kinase (United States Biomedical), [γ-^{32}P]ATP (MP Biomedicals, Solon, OH), and bicine. Labeling mixture was added to each sample and incubated for 45 min at 37 °C, followed by addition of apyrase for 30 min. at 37 °C. Thin layer chromatography (TLC) was then performed using methanol- washed cellulose PEI TLC plates (Selecto Scientific, Georgia, USA) with various plate orientations and solvents: to the origin in 1 M NaH_2PO_4 overnight, in opposite direction in 3.6 M lithium formate/8.5 M urea, 90° to the previous direction in 0.8 M LiCl/0.5 M Tris-Cl/8.5 M urea, and in same direction in 1.7 M NaH_2PO_4. Phosphorimaging was then used to measure the intensity of radioactive labeling. To determine the ratio of DNA adducts to normal nucleotides, normal nucleotides were also imaged. This was done by incubating a portion of the digested DNA with labeling mixture for 45 min at 37 °C, followed by TLC using LiCl solvent. Phosphorimaging was used to visualize the total nucleotides and DNA adducts on each TLC plate. Phosphorimaging software was used to measure the density of the corresponding spots for each sample. The relative adduct labeling was then determined by dividing the density of the adducted nucleotides by that of the total nucleotides for the same plate.

2.9. Immunohistochemistry

Paraformaldehyde-fixed cryosections were immunostained with primary antibodies directed against PCNA (Santa Cruz Biotechnology, #SC-56 at a dilution of 1:1500) using the MOM Immunodetection Kit (Vector Laboratories, Burlingame, CA). Antigen retrieval was first performed by incubating slides in 10 mM citrate buffer for 10 min at 95 °C, followed by blocking with MOM Mouse Ig Blocking Reagent, then Avidin/Biotin blocking, incubation with blocking serum, incubation with primary antibody, incubation with biotinylated anti-mouse Ig, blocking with 3% hydrogen peroxide in PBS, incubation with Vectastain ABC reagent, DAB conversion, and counterstaining. Negative controls included slides incubated with non-immune mouse IgG in place of primary antibody.

2.10. Terminal deoxynucleotidyl transferase-mediated dUTP nick end-labeling (TUNEL)

Paraformaldehyde-fixed cryosections were used for in situ detection of DNA fragmentation by the TUNEL method using the In Situ Cell Death Detection Kit POD (Roche) as previously described [56,64].

2.11. Quantification of TUNEL and immunostaining

All counting was conducted by an observer blind to genotype and treatment using light microscopy. Secondary and antral follicles were counted if the oocyte was present in a section for a total of 4–16 sections per animal. Follicles were considered TUNEL-positive if there were 3 or more TUNEL-positive granulosa cells per cross-section. The total number of TUNEL-positive and negative secondary and antral follicles was counted for each section. The average percentage of positive secondary and antral follicles was then calculated for each mouse and was used for statistical analyses.

For counting of PCNA or TUNEL positive OSE cells, a site lying above a growing follicle was chosen and considered an over-site. The total numbers of positive and negative OSE cells in the over-site were counted in one 400× microscope field. After an over-site was counted for a section, a site 180° away from the over-site was found that contained OSE between two growing follicles. This site was called the adjacent site. For the next section, the first site to be located would be an adjacent site, and following that would be an over-site 180° away. 8 to 20 sections were counted per experimen-

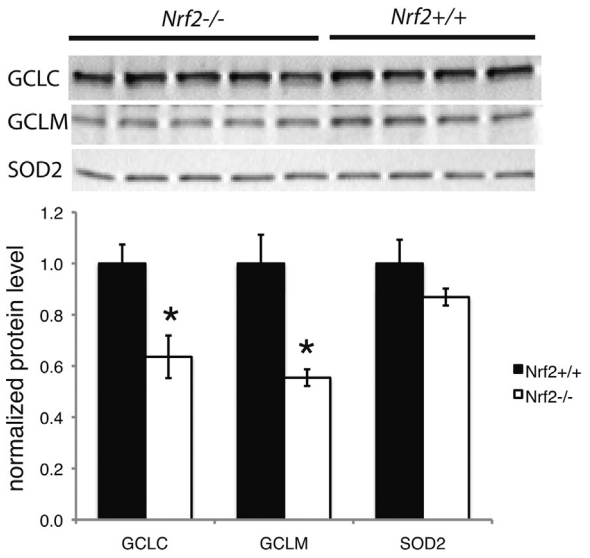

Fig. 1. Protein levels of GCLC and GCLM, but not SOD2 are decreased in ovaries of *Nrf2*−/− mice compared to *Nrf2*+/+ mice. Ovaries of *Nrf2*−/− and *Nrf2*+/+ mice were processed for immunoblotting as described in Section 2. Images of blots are shown at top. The graph shows mean ± SEM densitometry of protein of interest normalized to β-actin loading control. $N = 4–5$/group. $^{*}P < 0.05$ versus *Nrf2*+/+ by *t*-test.

tal animal per experiment to determine the numbers of PCNA or TUNEL positive OSE cells. There were 3–4 experimental animals per group for TUNEL and PCNA-immunostaining. The average percentage of positive cells per animal was calculated, and these averages were used for statistical analyses.

2.12. Statistics

Continuous dependent variables with homogenous variances were analyzed by ANCOVA with independent variables genotype and covariate BaP dose or by *t*-test, as appropriate. When variances were not homogeneous non-parametric tests were used. Data expressed as fractions or percentages (fraction of atretic, TUNEL positive or PCNA positive follicles or OSE cells) were subjected to arcsine square root transformation prior to analysis [65].

3. Results

3.1. Effect of Nrf2 deletion on ovarian GSH synthesis and antioxidant gene expression

Total ovarian GSH concentrations in *Nrf2*−/− females were about 15% lower than in *Nrf2*+/+ females (2.7 ± 0.15 nmol GSH/mg ovary compared to 3.2 ± 0.13 nmol GSH/mg ovary, respectively; $P < 0.05$ by *t*-test). A similar, although not statistically significant, trend was observed when GSH concentrations were expressed in terms of protein content (57 ± 4.7 nmol GSH/mg protein in *Nrf2*−/− versus 67 ± 6.9 nmol GSH/mg protein in *Nrf2*+/+, $P = 0.245$ by *t*-test). Consistent with the lower GSH concentrations, *Nrf2*−/− ovaries also had lower protein levels of the catalytic and modifier subunits of GCL, the rate-limiting enzyme in GSH synthesis. Compared to *Nrf2*+/+ ovaries, *Nrf2*−/− ovaries had 36% lower protein levels of GCLC ($P = 0.017$) and 45% lower protein levels of GCLM ($P = 0.024$; Fig. 1). In contrast, ovarian SOD2 (also called Mn-SOD) protein levels were not affected by lack of *Nrf2* (Fig. 1).

Ovarian mRNA levels of genes involved in BaP metabolism were measured in *Nrf2*−/− and *Nrf2*+/+ mice (Table 1). Ovarian mRNA levels of *Gstm1* ($P = 0.006$ by *t*-test) and *Ephx1* ($P = 0.07$) were 67% and 91% lower, respectively, in *Nrf2*−/− than in *Nrf2*+/+ mice. When the *Ephx1* outlier that fell outside of the 95% confidence interval for the *Nrf2*+/+ group was excluded, the effect of *Nrf2* genotype was statistically significant ($P = 0.021$). Ovarian mRNA levels of *Gstm2* and *Gsta4* were 36% and 54% lower, respectively, in the *Nrf2*−/− mice, but the differences were not statistically significant. The mRNA levels of *Gclc*, *Gclm*, and *Gstp1* did not differ between *Nrf2*−/− and *Nrf2*+/+ ovaries.

Table 1
Effects of Nrf2 deletion on ovarian expression of metabolic genes.

	Nrf2+/+	*Nrf2*−/−
Gclc	1.00 ± 0.13	0.79 ± 0.27
Gclm	1.00 ± 0.18	0.90 ± 0.25
Gstm1*	1.00 ± 0.14	0.34 ± 0.08
Gstm2	1.00 ± 0.16	0.64 ± 0.29
Gsta4	1.00 ± 0.26	0.46 ± 0.10
Gstp1	1.00 ± 0.22	1.04 ± 0.14
Ephx1**	1.00 ± 0.38	0.11 ± 0.05

$N = 4–5$/group.
* $P = 0.006$, *t*-test.
** $P = 0.07$, *t*-test.

3.2. Nrf2−/− mice are not more sensitive to the ovarian toxicity of BaP than Nrf2+/+ mice

As expected, BaP treatment caused statistically significant dose-dependent declines in the total numbers of healthy follicles per ovary (Fig. 2A) and the numbers of healthy primordial and primary follicles per ovary (Fig. 2B,C). The numbers of healthy secondary (Fig. 2D) and antral follicles (Fig. 2E) also decreased with BaP dose, but the effects were not statistically significant. The effects of *Nrf2* genotype on numbers of primordial, primary, secondary, or total healthy follicles were not statistically significant; however, *Nrf2*−/− mice had significantly greater numbers of multiovular follicles and fewer healthy antral follicles regardless of BaP dose (Fig. 2E,F).

No statistically significant *Nrf2* genotype- or BaP treatment-related differences in the percentages of TUNEL-positive, apoptotic secondary or antral follicles were observed (data not shown).

3.3. Effects of Nrf2 genotype and BaP treatment on ovarian DNA adducts

Nrf2+/+ and *Nrf2*−/− mice treated with 50 mg/kg BaP had two or three distinct ovarian DNA adducts as demonstrated by ^{32}P-postlabeling (Fig. 3), whereas no adducts were observed in DNA from ovaries of control, vehicle-treated mice (not shown). However, DNA adduct levels were not greater in ovaries from *Nrf2*−/− mice treated with BaP (Fig. 3C,D) compared to *Nrf2*+/+, BaP-treated mice (Fig. 3A,B). The relative levels of adducts in *Nrf2*−/− versus *Nrf2*+/+ ovaries were 0.8 for adduct 2 and 0.7 for adduct 3 (mean of two samples per genotype).

3.4. Effects of Nrf2 genotype and BaP treatment on ovarian surface epithelial (OSE) cell proliferation and apoptosis

Immunostaining for PCNA was used to detect OSE cell proliferation. PCNA positive and negative OSE cells located over antral follicles or away from antral follicles were counted and the percentages of positive cells were calculated. The percentages of PCNA positive OSE cells were lower in ovaries of BaP-treated mice. The effect of BaP dose on the percentage of PCNA positive OSE cells overlying antral follicles was statistically significant ($P = 0.018$; Fig. 4A), but the effect of BaP dose was not statistically significant for OSE cells not overlying antral follicles ($P = 0.286$; Fig. 4B). The effect of BaP dose was also statistically significant for all OSE cells combined

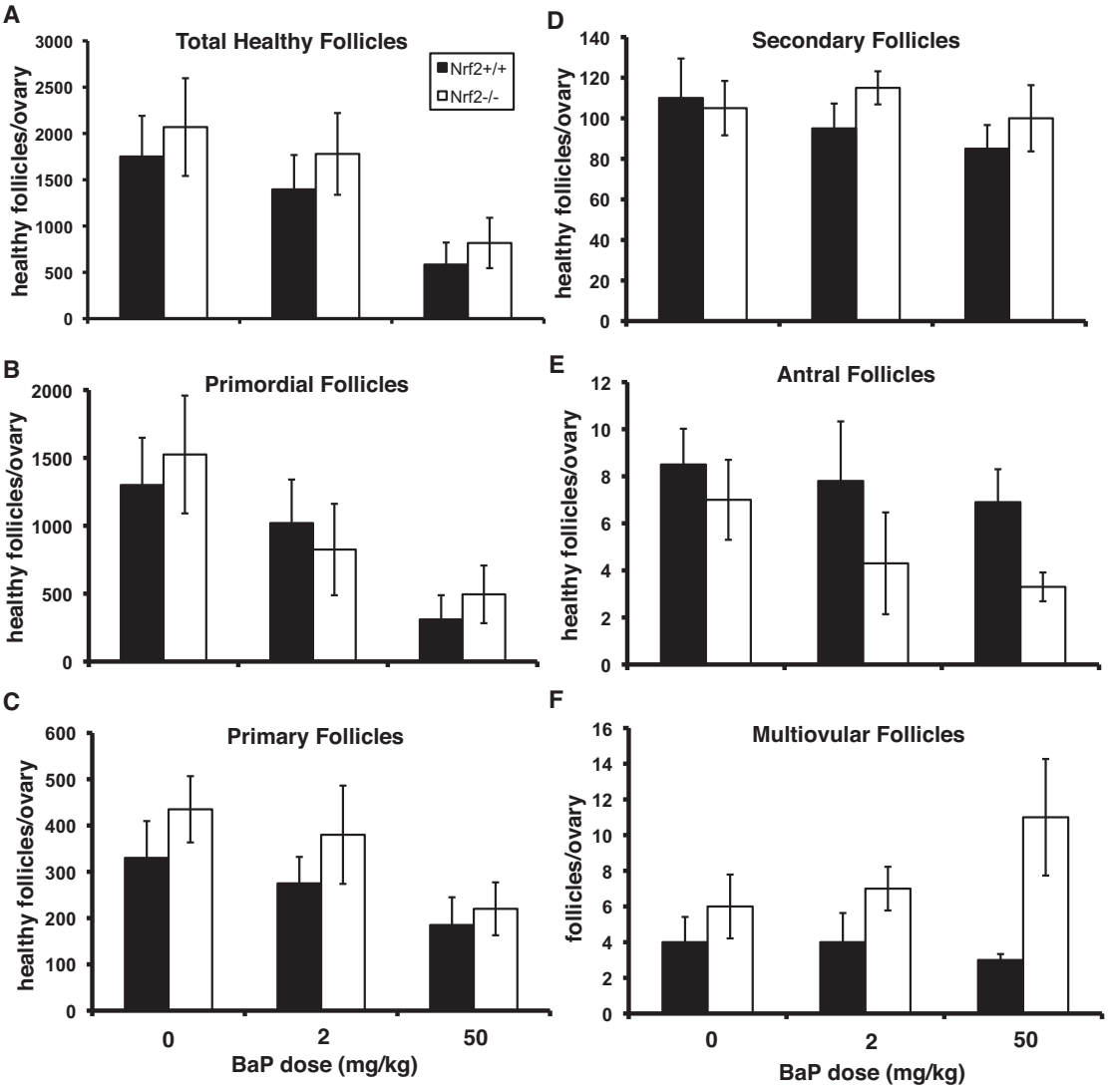

Fig. 2. Effects of *Nrf2* deletion and BaP treatment on numbers of healthy ovarian follicles.Graphs show mean ± SEM follicle counts. Data were analyzed by ANCOVA with BaP dose as a continuous variable and *Nrf2* genotype as a nominal variable. There was a BaP dose-dependent decrease in total healthy follicles (A) and healthy primordial follicles (B), $p = 0.001$, effect of BaP dose. There was no effect of genotype. (C) Healthy primary follicles also decreased with increasing BaP dose ($p = 0.020$). There was no effect of genotype. (D) Healthy secondary follicle numbers did not vary significantly with dose or genotype. (E) *Nrf2*−/− mice had fewer healthy antral follicles than their wild type littermates ($p = 0.037$). The effect of BaP treatment on antral follicle numbers was not statistically significant ($p = 0.23$). (F) *Nrf2*−/− ovaries had significantly greater numbers of multiovular follicles than wild type ovaries ($p = 0.045$, effect of genotype). There was no effect of BaP dose on multiovular follicles.

($P = 0.047$; Fig. 4C). The effect of *Nrf2* genotype was not statistically significant.

TUNEL was used to detect OSE cell apoptosis. TUNEL-positive and negative OSE cells located over antral follicles (data not shown), away from antral follicles (data not shown), or at all sites (Fig. 4D) were counted and the percentages of positive cells were calculated. Neither the effects of BaP dose nor the effects of *Nrf2* genotype were statistically significant.

3.5. *Nrf2* deletion accelerates the age-related decline in ovarian follicles

Follicle counts did not differ by *Nrf2* genotype in 35 day old mice, as described above (Fig. 2). However, we hypothesized that *Nrf2*−/− female mice, due to decreased ability to respond to oxidative stress, display a more rapid decline in follicle numbers with aging than *Nrf2+/+* mice. We therefore counted follicles in 10–12 month old (middle-aged) *Nrf2+/+* and *Nrf2*−/− mice. The results are shown in Fig. 5. Middle-aged *Nrf2*−/− female mice had statistically significantly fewer healthy primordial follicles ($P = 0.011$) than age-matched *Nrf2+/+* females, indicating greater depletion of the ovarian reserve in *Nrf2*−/− mice.

4. Discussion

NRF2 is a master regulator of the antioxidant response and serves as a key sensor detecting chemical-induced toxicity in various organs, including ovary [38,39]. In the presence of oxidative stress, the affinity of KEAP-1 for cytosolic NRF2 decreases, which promotes relocation of cytosolic NRF2 to the nucleus, where it induces the expression of target antioxidant genes, including GSTs and GSH synthesis genes [34–36]. The lack of NRF2 disrupts antioxidant signaling, leading to a decreased ability to mount an antioxidant defense [34,42] and decreased ability to metabolize xenobiotics, such as PAHs [37,66,67]. In the present study, *Nrf2*−/− female mice had similar numbers of ovarian follicles to *Nrf2+/ +* mice at 35 days of age, but *Nrf2*−/− mice had fewer remaining primordial follicles at 10–12 months of age compared

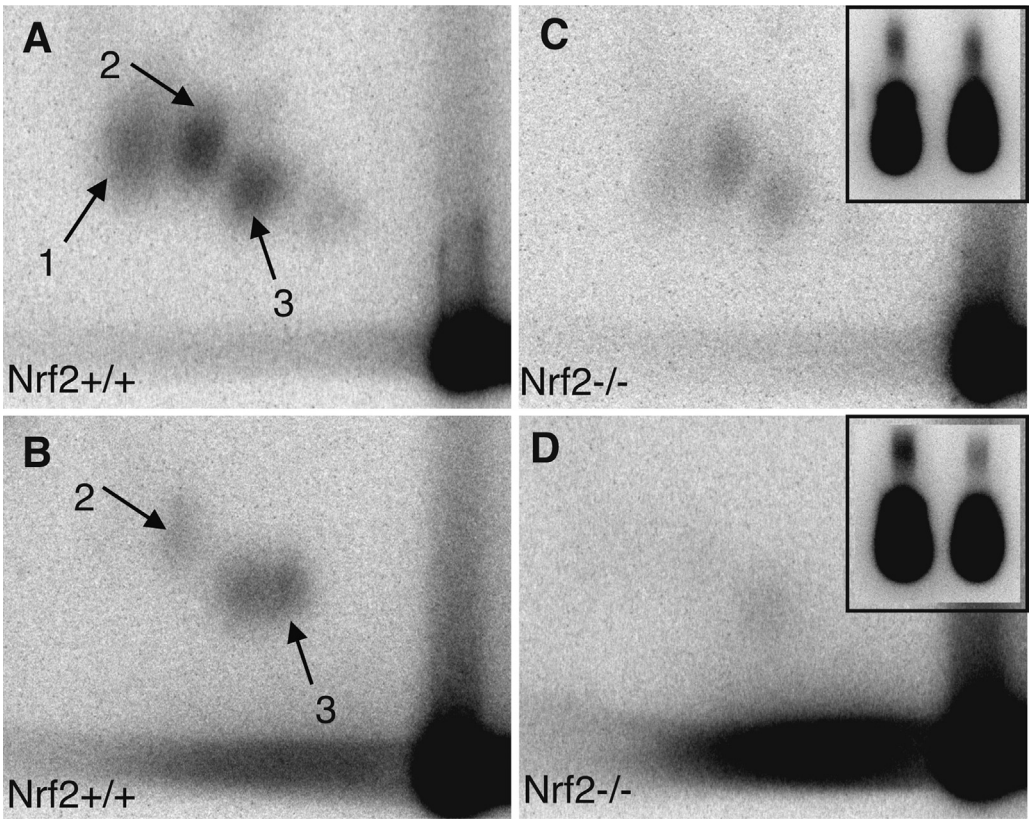

Fig. 3. Representative images of ^{32}P-postlabeling detection of DNA adducts in ovaries 7 days after i.p. injection with 50 mg/kg BP on postnatal day 28 of *Nrf2+/+* (A,B) or *Nrf2−/−* (C,D) mice. Three adducts are clearly visible (1–3) in A and C, while only two adducts are visible in B and D. The insets show total nucleotides for each TLC plate, with the total nucleotides for the *Nrf2+/+* ovary on the left and the *Nrf2−/−* ovary on the right. ^{32}P-postlabeling and TLC of A and C were performed on the same day and B and D were performed on a different day.

to *Nrf2+/+* littermates. This may indicate that sustained oxidative stress during aging accelerates depletion of primordial follicles in the middle-aged *Nrf2−/−* female mice. In contrast, our results show that *Nrf2−/−* mice do not have greater sensitivity to the ovarian toxicity induced by treatment with the PAH BaP.

GSTs are a major group of Phase II detoxification enzymes induced by NRF2 activation, and GST-catalyzed conjugation with GSH is an important Phase II biotransformation pathway for diol epoxide, diol, and quinone metabolites of PAHs [33]. GSH also detoxifies ROS produced as a result of BaP metabolism. We therefore hypothesized that *Nrf2−/−* mice, having decreased ovarian expression of several GSH-related genes would have increased ovarian sensitivity to BaP. We observed decreased mRNA levels of several GST genes, decreased protein expression of GCLC and GCLM, and decreased GSH concentrations in *Nrf2−/−* ovaries. However, in contrast to their reportedly greater sensitivity to the ovarian toxicant vinylcyclohexene diepoxide [38], *Nrf2−/−* mice did not have increased sensitivity to ovarian follicle destruction by BaP. In addition, ovarian BaP-related DNA adduct formation was not increased in the ovaries of *Nrf2−/−* mice compared to *Nrf2+/+* littermates. This may reflect the greater importance of downregulation of *Ephx1*, which is required to generate the reactive diol epoxide metabolite of BaP [24], than downregulation of GSTs and GSH, which detoxify BaP metabolites [33]. Indeed, ovarian mRNA levels of *Ephx1* in *Nrf2−/−* mice were less than 15% of those in *Nrf2+/+* mice, and *Ephx1* null mice are resistant to PAH-induced carcinogenesis [68]. The absence of BaP treatment-related increases in the percentages of apoptotic follicles or ovarian surface epithelial cells in mice of either *Nrf2* genotype in the present study are consistent with apoptotic cells having already been cleared by 7 days after BaP treatment.

BaP or its metabolites have been reported to stimulate proliferation of cultured breast epithelial cells and breast cancer cells via estrogen receptor dependent mechanisms [21,22,69,70] BaP treatment was shown to induce anchorage independent growth of normal human OSE cells that overexpressed CYP1A1 [71]. In contrast to these in vitro findings, we did not observe increased OSE proliferation after in vivo treatment with BaP measured by PCNA immunostaining 7 days after BaP injection. Rather, we observed decreased percentages of PCNA positive OSE cells after BaP treatment.

We and others have shown that ovarian aging is associated with decreased ovarian antioxidant defense capacity and increased oxidative damage [44–46,72–74]. We have also shown that *Nrf2−/−* male mice have normal spermatogenesis as young adults, but subsequently demonstrate an age-related decline in spermatogenesis, which is associated with testicular oxidative damage [43]. NRF2 is activated by ROS, and the activation of NRF2-dependent antioxidant signaling is an adaptive response to oxidative stress [67,75]. Thus NRF2 signaling may have important implications in countering aging in the ovary. In the present study, we observed downregulation of key antioxidants in *Nrf2−/−* ovaries. We found that *Nrf2−/−* mice had similar numbers of ovarian follicles at 35 days of age, but fewer follicles at 10–12 months of age compared to *Nrf2+/+* littermates. This is consistent with an accelerated age-related decline in ovarian follicle numbers in the *Nrf2−/−* mice. The accelerated decline in the total number of healthy follicles in *Nrf2−/−* mice was driven by a more rapid decline in the numbers of quiescent primordial follicles, which constitute the ovarian reserve. We recently reported an accelerated age- related decline in ovarian follicle numbers in another mouse model genetically deficient

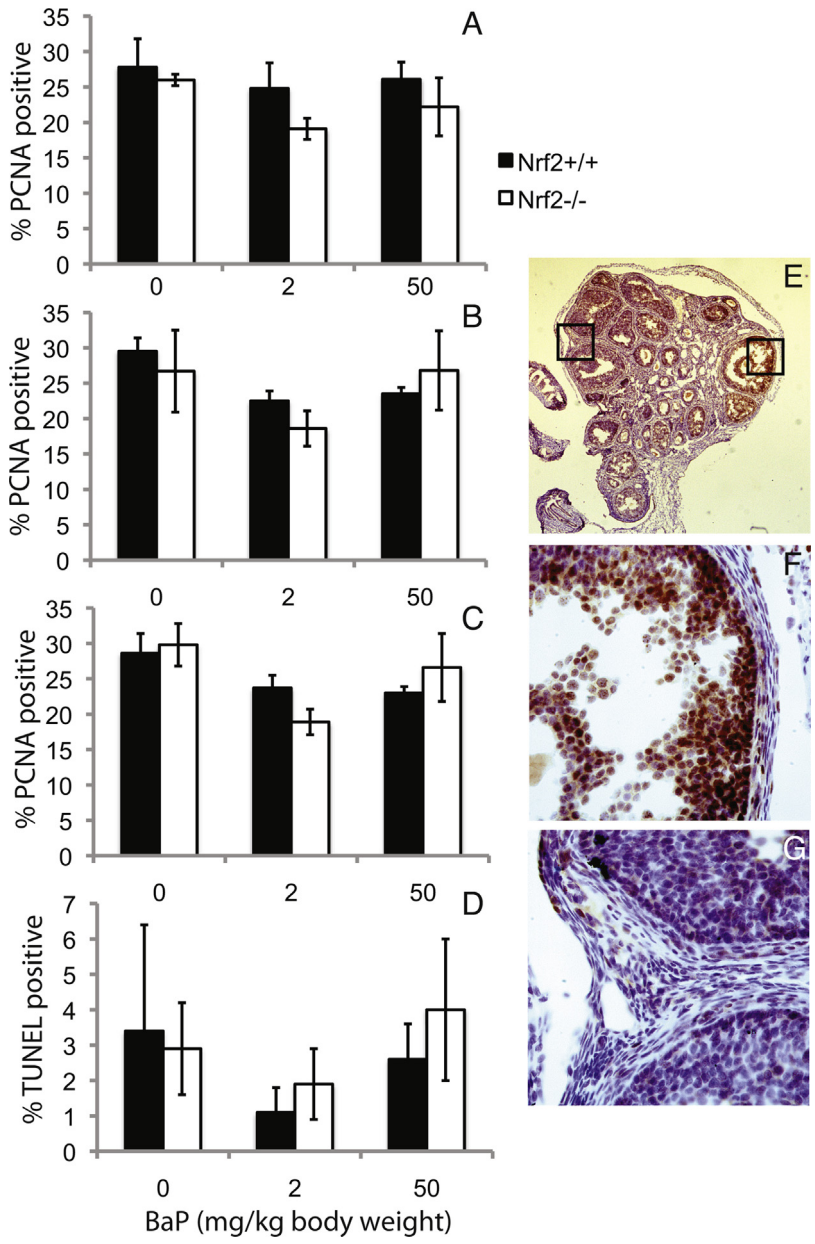

Fig. 4. Effects of BaP treatment and *Nrf2* deletion on ovarian surface epithelial cell proliferation and apoptosis. (A) Mean ± SEM percentage of PCNA positive OSE cells in site located over an antral follicle, as shown in F. Statistical analyses were performed by ANCOVA as for Fig. 2. The effect of BaP dose was statistically significant, $P = 0.018$; the effect of genotype was not. (B) Mean ± SEM percentage of PCNA positive OSE cells in site not located over an antral follicle, as shown in G. There were no statistically significant effects of BaP or genotype. (C) Mean ± SEM percentage of PCNA positive OSE cells overall. The effect of BaP dose was statistically significant, $P = 0.047$; the effect of genotype was not. (D) Mean ± SEM percentage of TUNEL positive OSE cells. (E) View of an entire ovarian section after PCNA immunostaining. Original magnification, 40×. F and G show higher magnification (400×) views of the areas indicated by squares in E.

in a key antioxidant gene, glutamate cysteine ligase modifier subunit (*Gclm*), a subunit of the rate limiting enzyme in GSH synthesis [47]. *Gclm*−/− mice have greatly decreased ovarian GSH concentrations and ratio of reduced to oxidized glutathione and increased ovarian oxidative protein and lipid damage, consistent with ovarian oxidative stress. Our current findings raise the possibility that NRF2 signaling is required for resistance to oxidative stress during aging in the ovary. Together our results from these two mouse models provide strong support for the hypothesis that increased ovarian oxidative stress can cause premature ovarian senescence.

We observed significantly more multiovular follicles in ovaries of *Nrf2*−/− mice than *Nrf2*+/+ mice at 35 days of age. Multiovular follicles are thought to arise due to incomplete oocyte cyst breakdown during primordial follicle formation [76]. Previous studies have shown that neonatal treatment with estradiol or with the soy isoflavone and phytoestrogen genistein increases the numbers of multiovular follicles [77]. Fetal exposure to gamma-radiation has been reported to increase multiovular follicle formation in rats [78]. Ionizing radiation is well known to cause oxidative stress [79,80], suggesting that oxidative stress may disrupt oocyte cyst breakdown leading to multiovular follicle formation.

In conclusion, our results show that *Nrf2*−/− and *Nrf2*+/+ mice have similar numbers of ovarian follicles at 35 days of age. However, by 10–12 months of age, the remaining primordial follicle pool is significantly smaller in *Nrf2*−/− compared to *Nrf2*+/+ mice, consistent with accelerated ovarian aging in *Nrf2*−/− mice. We also showed the ovarian concentrations of GSH and protein levels of the subunits of the rate-limiting enzyme in GSH synthesis

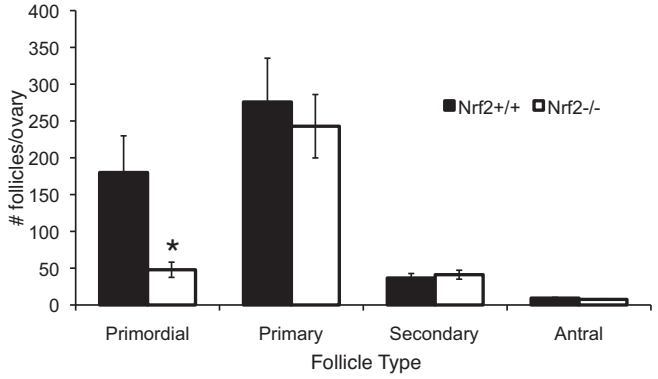

Fig. 5. Middle-aged *Nrf2*−/− mice have fewer ovarian follicles than *Nrf2*+/+ mice of the same age. Healthy primordial, primary, secondary, and antral follicles were counted as described in Section 2 in ovaries from 10 to 12 month old *Nrf2*−/− and *Nrf2*+/+ mice. The graph shows mean ± SEM follicles in each category per ovary. * $P < 0.02$ versus *Nrf2*+/+ by Mann–Whitney test. $N = 2$ twelve month old and $N = 4$ ten month old mice of each genotype.

are decreased in *Nrf2*−/− mice. Messenger RNA levels of several GSTs and of *Ephx1*, which are involved in BaP metabolism, are also decreased in *Nrf2*−/− ovaries. Unlike their reportedly greater sensitivity to the ovarian toxicity of vinylcyclohexene diepoxide, *Nrf2*−/− mice do not have increased sensitivity to the ovarian toxicity of BaP. This may be due to lower ovarian expression of *Ephx1* in *Nrf2*−/− mice, which is required to generate the toxic diol epoxide metabolite of BaP, but is involved in detoxification of vinylcyclohexene diepoxide.

Conflict of interest

The authors declare that there are no conflicts of interest.

Transparency document

The http://dx.doi.org/10.1016/j.reprotox.2015.07.080 associated with this article can be found in the online version.

Acknowledgments

The authors thank Kira Pate for optimizing the ^{32}P-postlabeling, Lee Sutherland and Jeffrey Kim for preparation of histological specimens.

Supported by NIH K08ES10963, NIH R21AG032087 and NIH R01ES020454 (to UL); NIH P30CA062203, the University of California Irvine (UC Irvine) Chao Family Comprehensive Cancer Center; University of California CRCC Research Grant(to UL); and the Center for Occupational and Environmental Health, UC Irvine.

Appendix A. Supplementary data

Supplementary data associated with this article can be found, in the online version, at http://dx.doi.org/10.1016/j.reprotox.2015.07.080

References

[1] D.R. Shopland, D.M. Burns, N.L. Benowitz, R.H. Amacher, Risks Associated with Smoking Cigarettes with Low Machine-Measured Yields of Tar and Nicotine, Smoking and Tobacco Control Monographs: U.S. Department of Health and Human Services, Public Health Service, National Institutes of Health, National Cancer Institute, 2001, pp. 1–236.
[2] ATSDR, Toxicological Profile for Polycyclic Aromatic Hydrocarbons, US Department of Health and Human Services, Public Health Service, Agency for Toxic Substances and Disease Registry, Atlanta, GA, 1995.
[3] C.A. Menzie, B.B. Potocki, J. Santodonato, Ambient concentrations and exposure to carcinogenic PAHs in the environment, Environ. Sci. Technol. 26 (1992) 1278–1284.
[4] D.D. Baird, A.J. Wilcox, Cigarette smoking associated with delayed conception, JAMA 253 (1985) 2979–2983.
[5] E. Alderete, B. Eskenazi, R. Sholtz, Effect of cigarette smoking and coffee drinking on time to conception, Epidemiology 6 (1995) 403–408.
[6] T.K. Jensen, T.B. Henriksen, N.H. Hjollund, T. Scheike, H. Kolstad, A. Giwercman, et al., Adult and prenatal exposures to tobacco smoke as risk indicators of fertility among 430 Danish couples, Am. J. Epidemiol. 148 (1998) 992–997.
[7] D.R. Mattison, D.R. Plowchalk, M.J. Meadows, M.M. Miller, A. Malek, S. London, The effect of smoking on oogenesis, fertilization, and implantation, Semin. Reprod. Endocrinol. 7 (1989) 291–304.
[8] B.L. Harlow, L.B. Signorello, Factors associated with early menopause, Maturitas 35 (2000) 3–9.
[9] D.R. Mattison, Difference in sensitivity of rat and mouse primordial oocytes to destruction by polycyclic aromatic hydrocarbons, Chem. Biol. Interact. 28 (1979) 133–137.
[10] D.R. Mattison, M.S. Nightingale, Oocyte destruction by polycyclic aromatic hydrocarbons is not linked to the inducibility of ovarian aryl hydrocarbon (benzo(a) pyrene) hydroxylase activity in (DBA/2N x C57BL/6N) F1 x DBA/2N backcross mice, Pediatr. Pharmacol. 2 (1982) 11–21.
[11] D.R. Mattison, S.S. Thorgeirsson, Ovarian aryl hydrocarbon hydroxylase activity and primordial oocyte toxicity of polycyclic aromatic hydrocarbons in mice, Cancer Res. 39 (1979) 3471–3475.
[12] D.R. Mattison, N.B. White, M.R. Nightingale, The effect of benzo(a) pyrene on fertility, primordial oocyte number, and ovarian response to pregnant mare's serum gonadotropin, Pediatr. Pharmacol. 1 (1980) 143–151.
[13] S.M. Borman, P.J. Christian, I.G. Sipes, P.B. Hoyer, Ovotoxicity in female Fischer rats and B6 mice induced by low-dose exposure to three polycyclic aromatic hydrocarbons: comparison through calculation of an ovotoxic index, Toxicol. Appl. Pharmacol. 167 (2000) 191–198.
[14] T. Matikainen, G.I. Perez, A. Jurisicova, J.K. Pru, J.J. Schlezinger, H.-Y. Ryu, et al., Aromatic hydrocarbon receptor-driven Bax gene expression is required for premature ovarian failure caused by biohazardous environmental chemicals, Nat. Genet. 28 (2001) 355–360.
[15] O. Taguchi, S.D. Michael, Y. Nishizuka, Rapid induction of ovarian granulosa cell tumors by 7,2-dimethylbenz(a) anthracene in neonatally estrogenized mice, Cancer Res. 48 (1988) 425–429.
[16] L.E. Shorey, D.J. Castro, W.M. Baird, L.K. Siddens, C.V. Löhr, M.M. Matzke, et al., Transplacental carcinogenesis with dibenz[*def*,*p*]chrysene (DBC): timing of maternal exposures determines target tissue response in offspring, Cancer Lett. 317 (2012) 49–55.
[17] J. Lim, G.W. Lawson, B.N. Nakamura, L. Ortiz, J.A. Hur, T.J. Kavanagh, et al., Glutathione-deficient mice have increased sensitivity to transplacental benzo[a]pyrene- induced premature ovarian failure and ovarian tumorigenesis, Cancer Res. 73 (2013) 908–917.
[18] V.W. Chen, B. Ruiz, J.L. Killeen, T.R. Cote, X.C. Wu, C.N. Correa, Pathology and classification of ovarian tumors, Cancer 97 (2003) 2631–2642.
[19] A. Flesken-Nikitin, C.-I. Hwang, C.-Y. Cheng, T.V. Michurina, G. Enikolopov, A.Y. Nikitin, Ovarian surface epithelium at the junction area contains a cancer-prone stem cell niche, Nature 495 (2013) 241–245.
[20] S.L. Tannheimer, S.P. Ethier, K.K. Caldwell, S.W. Burchiel, Benzo[a]pyrene and TCDD-induced alterations in tyrosine phosphorylation and insulin-like growth factor signaling pathways in the MCF-7a human mammary epithelial cell line, Carcinogenesis 19 (1998) 1291–1297.
[21] S.L. Tannheimer, S.L. Barton, S.P. Ethier, S.W. Burchiel, Carcinogenic polycyclic aromatic hydrocarbons increase intracellular Ca2+ and cell proliferation in primary human mammary epithelial cells, Carcinogenesis 18 (1997) 1177–1182.
[22] M. Plíšková, J. Vondráček, B. Vojtěšek, A. Kozubík, M. Machala, Deregulation of cell proliferation by polycyclic aromatic hydrocarbons in human breast carcinoma MCF-7 cells reflects both genotoxic and nongenotoxic events, Toxicol. Sci. 83 (2005) 246–256.
[23] H.E. Kleiner, S. Vulimiri, W.B. Hatten, M.J. Reed, D.W. Nebert, C.R. Jefcoate, et al., Role of cytochrome P4501 family members in the metabolic activation of polycyclic aromatic hydrocarbons in mouse epidermis, Chem. Res. Toxicol. 17 (2004) 1667–1674.
[24] W. Xue, D. Warshawsky, Metabolic activation of polycyclic aromatic hydrocarbon and heterocyclic aromatic hydrocarbons and DNA damage: a review, Toxicol. Appl. Pharmacol. 206 (2005) 73–93.
[25] K. Takizawa, H. Yagi, D.M. Jerina, D.R. Mattison, Murine strain differences in ovotoxicity following intraovarian injection with benzo(*a*) pyrene, (+)-(7*R*,8*S*)-oxide, (−)- (7*R*,8*S*)-dihydrodiol, or (+)-(7*R*,8*S*)-diol-(9*S*,10*R*)-epoxide-2, Cancer Res. 44 (1984) 2571–2576.
[26] E.A. Cannady, C.A. Dyer, P.J. Christian, I.G. Sipes, P.B. Hoyer, Expression and activity of microsomal epoxide hydrolase in follicles isolated from mouse ovaries, Toxicol. Sci. 68 (2002) 24–31.
[27] J.K. Coller, P. Fritz, U.M. Zanger, I. Siegle, M. Eichelbaum, H.K. Kroemer, et al., Distribution of microsomal epoxide hydrolase in humans: an immunohistochemical study in normal tissues, and benign and malignant tumours, Histochem. J. 33 (2001) 329–336.
[28] L.N. Springer, M.E. McAsey, J.A. Flaws, J.L. Tilly, I.G. Sipes, P.B. Hoyer, Involvement of apoptosis in 4-vinylcyclohexene diepoxide-induced ovotoxicity in rats, Toxicol. Appl. Pharmacol. 139 (1996) 394–401.

[29] T. Shimada, A. Sugie, M. Shindo, T. Nakajima, E. Azuma, M. Hashimoto, et al., Tissue-specific induction of cytochromes P450 1A1 and 1B1 by polycyclic aromatic hydrocarbons and polychlorinated biphenyls in engineered C57BL/6J mice of *arylhydrocarbon receptor* gene, Toxicol. Appl. Pharmacol. 187 (2003) 1–10.
[30] S. Otto, K.K. Bhattacharyya, C.R. Jefcoate, Polycyclic aromatic hydrocarbon metabolism in rat adrenal, ovary, and testis microsomes is catalyzed by the same novel cytochrome P450 (P450RAP), Endocrinology 131 (1992) 3067–3076.
[31] L. Muskhelishvili, P.A. Thompson, D.F. Kusewitt, C. Wang, F.F. Kadlubar, In situ hybridization and immunohistochemical analysis of cytochrome P450 1B1 expression in human normal tissues, J. Histochem. Cytochem. 49 (2001) 229–236.
[32] K.K. Bhattacharyya, P.B. Brake, S.E. Eltom, S.A. Otto, C.R. Jefcoate, Identification of a rat adrenal cytochrome P450 active in polycyclic aromatic hydrocarbon metabolism as rat CYP1B1, J. Biol. Chem. 270 (1995) 11595–11602.
[33] A. Seidel, T. Friedberg, B. Löllman, A. Schwierzok, M. Funk, H. Frank, et al., Detoxification of optically active bay- and fjord-region polycyclic aromatic hydrocarbon dihydrodiol epoxides by human glutathione transferase P 1-1 expressed in Chinese hamster V79 cells, Carcinogenesis 19 (1998) 1975–1981.
[34] J.Y. Chan, M. Kwong, Impaired expression of glutathione synthetic enzyme genes in mice with targeted deletion of the Nrf2 basic-leucine zipper protein, Biochim. Biophys. Acta 1517 (2000) 19–26.
[35] M. Ramos-Gomez, P.M. Dolan, K. Itoh, M. Yamamoto, T.W. Kensler, Interactive effects of nrf2 genotype and oltipraz on benzo[a]pyrene DNA adducts and tumor yield in mice, Carcinogenesis 24 (2003) 461–467.
[36] H. Zhu, K. Itoh, M. Yamamoto, J.L. Zweier, Y. Li, Role of Nrf2 signaling in regulation of antioxidants and phase 2 enzymes in cardiac fibroblasts: protection against reactive oxygen and nitrogen species-induced cell injury, FEBS Lett. 579 (2005) 3029–3036.
[37] M. Ramos-Gomez, M.-K. Kwak, P.M. Dolan, K. Itoh, M. Yamamoto, P. Talalay, et al., Sensitivity to carcinogenesis is increased and chemoprotective efficacy of enzyme inducers is lost in *nrf2* transcription factor-deficient mice, Proc. Natl. Acad. Sci. U. S. A. 98 (2001) 3410–3415.
[38] X. Hu, J.R. Roberts, P.L. Apopa, Y.W. Kan, Q. Ma, Accelerated ovarian failure induced by 4-vinyl cyclohexene diepoxide in Nrf2 null mice, Mol. Cell. Biol. 26 (2006) 940–954.
[39] K. Chan, X.-D. Han, Y.W. Kan, An important function of Nrf2 in combating oxidative stress: detoxification of acetaminophen, Proc. Natl. Acad. Sci. U. S. A. 98 (2001) 4611–4616.
[40] J.-M. Lee, K. Chan, Y.W. Kan, J.A. Johnson, Targeted disruption of Nrf2 causes regenerative immune-mediated hemolytic anemia, Proc. Natl. Acad. Sci. U. S. A. 101 (2004) 9751–9756.
[41] Q. Ma, L. Battelli, A.F. Hubbs, Multiorgan autoimmune inflammation, enhanced lymphoproliferation, and impaired homeostasis of reactive oxygen species in mice lacking the antioxidant- activated transcription factor *Nrf2*, Am. J. Pathol. 168 (2006) 1960–1974.
[42] L. Leung, M. Kwong, S. Hou, C.J. Lee, J.Y. Chan, Deficiency of the Nrf1 and Nrf2 transcription factors results in early embryonic lethality and severe oxidative stress, J. Biol. Chem. 278 (2003) 48021–48029.
[43] B.N. Nakamura, G. Lawson, J.Y. Chan, J. Banuelos, M.M. Cortés, Y.D. Hoang, et al., Knockout of the transcription factor *Nrf2* disrupts spermatogenesis in an age-dependent manner, Free Radic. Biol. Med. 49 (2010) 1368–1379.
[44] J. Lim, U. Luderer, Oxidative damage increases and antioxidant gene expression decreases with aging in the mouse ovary, Biol. Reprod. 84 (2011) 775–782.
[45] J.J. Tarín, Potential effects of age-associated oxidative stress on mammalian oocytes/embryos, Mol. Hum. Reprod. 2 (1996) 717–724.
[46] T. Hamatani, G. Falco, M.G. Carter, H. Akutsu, C.A. Stagg, A.A. Sharov, et al., Age- associated alteration of gene expression patterns in mouse oocytes, Hum. Mol. Genet. 13 (2004) 2263–2278.
[47] J. Lim, B.N. Nakamura, I. Mohar, T.J. Kavanagh, U. Luderer, Glutamate cysteine ligase modifier subunit (*Gclm*) null mice have increased ovarian oxidative stress and accelerated age-related ovarian failure, Endocrinology 17 (June) (2015) (Epub ahead of print).
[48] K. Chan, R. Lu, J.C. Chang, Y.W. Kan, NRF2, a member of the NFE2 family of transcription factors, is not essential for murine erythropoiesis, growth, and development, Proc. Natl. Acad. Sci. U. S. A. 93 (1996) 13493–13948.
[49] NRC, Guide for the Care and Use of Laboratory Animals, National Research Council, National Academy of Sciences, Washington, D.C, 1996.
[50] M. Tsai-Turton, U. Luderer, Gonadotropin regulation of glutamate cysteine ligase catalytic and modifier subunit expression in the rat ovary is subunit and follicle stage-specific, Am. J. Physiol. 289 (2005) E391–E402.
[51] O.W. Griffith, Determination of glutathione and glutathione disulfide using glutathione reductase and 2-vinylpyridine, Anal. Biochem. 106 (1980) 207–212.
[52] U. Luderer, T.J. Kavanagh, C.C. White, E.M. Faustman, Gonadotropin regulation of glutathione synthesis in the rat ovary, Reprod. Toxicol. 15 (2001) 495–504.
[53] S.A. Thompson, C.C. White, C.M. Krejsa, D. Diaz, J.S. Woods, D.L. Eaton, et al., Induction of glutamate-cysteine ligase (γ-glutamylcysteine synthetase) in the brains of adult female mice subchronically exposed to methylmercury, Toxicol. Lett. 110 (1999) 1–9.
[54] M.W. Pfaffl, A new mathematical model for relative quantification in real-time RT-PCR, Nucleic Acids Res. 29 (2001) e45.
[55] K.J. Livak, T.D. Schmittgen, Analysis of relative gene expression data using real-time quantitative PCR and the $2^{-\Delta\Delta C}$T method, Methods 25 (2001) 402–408.
[56] S.G. Lopez, U. Luderer, Effects of cyclophosphamide and buthionine sulfoximine on ovarian glutathione and apoptosis, Free Radic. Biol. Med. 36 (2004) 1366–1377.
[57] T. Pedersen, H. Peters, Proposal for a classification of oocytes in the mouse ovary, J. Reprod. Fertil. 17 (1968) 555–557.
[58] D.R. Plowchalk, B.J. Smith, D.R. Mattison, Assessment of toxicity to the ovary using follicle quantitation and morphometrics, in: J.J. Heindel, R.E. Chapin (Eds.), Female Reproductive Toxicology, Academic Press, San Diego, CA, 1993, pp. 57–68.
[59] A.N. Hirshfield, Size-frequency analysis of atresia in cycling rats, Biol. Reprod. 38 (1988) 1181–1188.
[60] V.S. Ratts, J.A. Flaws, R. Kolp, C.M. Sorenson, J.L. Tilly, Ablation of bcl-2 gene expression decreases the numbers of oocytes and primordial follicles established in the post-natal female mouse gonad, Endocrinology 136 (1995) 3665–3668.
[61] K. Randerath, E. Randerath, ^{32}P-postlabeling methods for DNA adduct detection: overview and critical evaluation, Drug Metab. Rev. 26 (1994) 67–85.
[62] M.V. Reddy, K. Randerath, Nuclease P1-mediated enhancement of sensitivity of ^{32}P-postlabeling test for structurally diverse DNA adducts, Carcinogenesis 7 (1986) 1543–1551.
[63] K. Randerath, M.V. Reddy, R.C. Gupta, ^{32}P-labeling test for DNA damage, Proc. Natl. Acad. Sci. U. S. A. 78 (1981) 6126–6129.
[64] U. Luderer, D. Diaz, E.M. Faustman, T.J. Kavanagh, Localization of glutamate cysteine ligase subunit mRNA within the rat ovary and relationship to follicular atresia, Mol. Reprod. Dev. 65 (2003) 254–261.
[65] B.S. Pasternack, R.E. Shore, Analysis of dichotomous response data from toxicological experiments involving stable laboratory mouse populations, Biometrics 38 (1982) 1057–1067.
[66] Y. Aoki, A.H. Hashimoto, K. Amanuma, M. Matsumoto, K. Hiyoshi, H. Takano, et al., Enhanced spontaneous and benzo(a) pyrene-induced mutations in the lung of Nrf2-deficient *gpt* delta mice, Cancer Res. 67 (2007) 5643–5648.
[67] T.W. Kensler, N. Wakabayashi, Nrf2: friend or foe for chemoprevention? Carcinogenesis 31 (2010) 90–99.
[68] M. Miyata, G. Kudo, Y.-H. Lee, T.J. Yang, H.V. Gelboin, P. Fernandez-Salguero, et al., Targeted disruption of the microsomal epoxide hydrolase gene, J. Biol. Chem. 274 (1999) 23963–23968.
[69] M.M.H. van Lipzig, N.P.E. Vermeulen, R. Gusinu, J. Legler, H. Frank, A. Seidel, et al., Formation of estrogenic metabolites of benzo[a]pyrene and chrysene by cytochrome P450 activity and their combined and supra-maximal estrogenic activity, Environ. Toxicol. Pharmacol. 19 (2005) 41–55.
[70] A.D. Burdick, J.W.I. Davis, K.J. Liu, L.G. Hudson, H. Shi, M.L. Monske, et al., Benzo(a) pyrene quinones increase cell proliferation, generate reactive oxygen species, and transactivate the epidermal growth factor receptor in breast epithelial cells, Cancer Res. 63 (2003) 7825–7833.
[71] Y.-K. Leung, K.-M. Lau, J. Mobley, Z. Jiang, S.-M. Ho, Overexpression of cytochrome P450 1A1 and its novel spliced variant in ovarian cancer cells: alternative subcellular enzyme compartmentation may contribute to carcinogenesis, Cancer Res. 65 (2005) 3726–3734.
[72] Z. Wiener-Megnazi, L. Vardi, A. Lissak, S. Shnizer, A.Z. Reznick, D. Ishai, et al., Oxidative stress indices in follicular fluid as measured by the thermochemi-luminescence assay correlate with outcome parameters in in vitro fertilization, Fertil. Steril. 82 (Suppl. 3) (2004) 1171–1176.
[73] C. Tatone, M.C. Carbone, S. Falone, P. Aimola, A. Giardinelli, D. Caserta, et al., Age- dependent changes in the expression of superoxide dismutases and catalase are associated with ultrastructural modifications in human granulosa cells, Mol. Reprod. Dev. 12 (2006) 655–660.
[74] S. Das, R. Chattopadhyay, S. Ghosh, S. Ghosh, S.K. G, B.N. Chakravarty, et al., Reactive oxygen species level in follicular fluid–embryo quality marker in IVF? Hum. Reprod. 21 (2006) 2403–2407.
[75] M. Kobayashi, M. Yamamoto, Nrf2-Keap1 regulation of cellular defense mechanisms against electrophiles and reactive oxygen species, Adv. Enzyme Regul. 46 (2006) 113–140.
[76] M.E. Pepling, Follicular assembly mechanisms of action, Reproduction 143 (2012) 139–149.
[77] Y. Chen, W.N. Jefferson, R.R. Newbold, E. Padilla-Banks, M.E. Pepling, Estradiol, progesterone, and genistein inhibit oocyte nest breakdown and primordial follicle assembly in the neonatal mouse ovary in vitro and in vivo, Endocrinology 148 (2007) 3580–3590.
[78] S. Mazaud-Guittot, C.J. Guigon, N. Coudouel, S. Magre, Consequences of fetal irradiation on follicle histogenesis and early follicle development in rat ovaries, Biol. Reprod. 75 (2006) 749–759.
[79] J.F. Ward, The complexity of DNA Damage: relevance to biological consequences, Int. J. Radiat. Biol. 66 (1994) 427–432.
[80] P.A. Riley, Free radicals in biology: oxidative stress and the effects of ionizing radiation, Int. J. Radiat. Biol. 65 (1994) 27–33.